Observation of swallowtail catastrophe singularity in non-Hermitian bands and its topological origin

Jing Hu, Ruo-Yang Zhang, Yixiao Wang, Yifei Zhu*, Hongwei Jia†, C. T. Chan‡

Abstract: Exceptional surfaces in non-Hermitian band structures are singular hypersurfaces in parameter space. Hypersurface singularities can be folds, cusps and intersections, which play central roles in catastrophe theory. Here we propose that a three-band non-Hermitian system, being non-reciprocal and defined in three-dimensional space, exhibits swallowtail catastrophe singularity in band structures. We discover that cusps, intersections and isolated singular lines in the swallowtail correspond to exceptional lines of order three (EL3), non-defective intersection lines (NIL) of exceptional surfaces, and nodal lines (NL), respectively. Hence, the swallowtail is an interactive phenomenon within elementary types of degeneracy lines. To experimentally observe the interaction behaviour, we realize the model with a topological circuit by incorporating operational amplifiers, with the parameter space replaced with synthetic dimensions that can be associated with circuit elements. By characterizing the topology of the singularities with adiabatic transformation of eigenstates, we reveal that the swallowtail can emerge because these degeneracy lines are topologically associated with each other. Our finding constitutes the first observation and demonstration of swallowtail catastrophe in non-Hermitian bands, possibly opening new avenues for the design of systems realizing robust topological phases.

Introduction: Non-Hermiticity is ubiquitous in the real world because most systems are not isolated. Such systems are described by non-Hermitian Hamiltonians, with eigenenergies being complex [1,2,3,4,5,6,7,8,33], representing energy exchange with surrounding environments. Degeneracies in band structures are sometimes non-differentiable singularities, which are quite similar to topological defects in real space, carrying non-trivial topological invariants. Well-known singularities in Hermitian bands are Weyl/Dirac points and nodal lines [9,10,11,12,13,14,15,16,17,18,19], and their presence is often accompanied with exotic physical phenomena, such as bulk-edge correspondence [9,16,19] and chiral Landau levels [17]. While the complex nature of non-Hermitian bands result in more complicated singularities, i.e. the exceptional degeneracies, at which two or more eigenstates coalesce. Exceptional degeneracies can carry fractional topological invariants, which not only enriches the topology classes in band theories [2,4,6,7], but also induces more intriguing physical consequences, such as bulk Fermi arcs [4,7] and skin effects [20,21,22,23,24].

Surfaces of exceptional points in Non-Hermitian systems with parity-time (*PT*) inversion symmetry or chiral symmetry act as boundaries between real and imaginary line gaps, and are singular hypersurfaces in parameter space [25,26,27]. Higher order singularities on hypersurfaces can be folds, cusps and intersections, playing central roles in catastrophe theory [28]. The correspondences of cusps and intersections in band structures have been found as high order exceptional degeneracies [7,29], and non-defective intersection degeneracies [29,30], respectively. The various types of degeneracy lines in non-Hermitian bands bring possibilities that they can interact with each other. However, previous works are commonly based on a single type, and interactive behaviours within different types, as well as the underlying topological origin remain unexplored. Here, we show that a *PT* symmetric non-Hermitian three-band system, which is non-reciprocal and defined in three-dimensional (3D) parameter space, exhibits a swallowtail catastrophe singularity in the band structure. The swallowtail is an elementary catastrophe in ADE classifications [28,36,37], and was widely applied in mechanics [31] and caustics [32], but was never discovered in band structures before. For the first time, we reveal that the cusps, intersections and isolated singular lines on the swallowtail are exceptional lines of order three (EL3), non-defective intersection lines (NIL), and nodal lines (NL), respectively. Hence, the swallowtail catastrophe is an interactive phenomenon within the elementary degeneracy lines in non-Hermitian

bands. With an electric circuit model incorporating operational amplifier, we not only observed swallowtail catastrophe singularity, but also characterized the topology of these degeneracy lines with adiabatic transformation of eigenstates. We demonstrate theoretically and experimentally that the degeneracy lines are topologically associated with each other, protecting the emergence of the swallowtail.

The three-band Hamiltonian we consider takes the following form

$$H=\begin{pmatrix} -f_1-f_2+1 & -f_1 & -f_2 \\ f_1 & f_1+f_3 & -f_3 \\ f_2 & -f_3 & f_2+f_3 \end{pmatrix} \tag{1}$$

where f_1-f_3 are three degrees of freedom defining the 3D real parameter space. One finds that the Hamiltonian satisfies two Altland-Zirnbauer symmetries [1]

$$\eta H\eta^{-1}=H^{\dagger}, \quad [H,PT]=0 \tag{2}$$

Here η denotes the pseudo-Hermiticity operation that takes the Riemannian metric form $\eta=\mathrm{diag}(-1,1,1)$, and PT is the Parity-Time symmetric operator and can be treated as a complex conjugate. The non-Hermiticity comes from the anti-symmetry of the off-diagonal elements in the Hamiltonian, representing non-reciprocal hoppings between nodes. Degenerate surfaces and lines (obtained by solving zeros of the discriminant of characteristic polynomial) in the band structure are numerically shown in Fig. 1A, with the exceptional surfaces of order two (ES) denoted by the red surfaces. The NL and the NIL (blue lines) are both non-defective degeneracy lines (eigenstates are linearly independent of each other), and are two segments separated by the meeting point (MT, red star) in Fig. 1A. However, they are intrinsically different from each other, as the former is isolated from any ESs, but the latter is a complete intersection of ESs [30]. The MT simultaneously emits two EL3s (black lines), which are defective degeneracies (all three eigenstates coalesce) and are cusps of ESs. The overall geometric structure of the singularities (including degeneracy point, lines and surfaces) form a swallowtail catastrophe. It can be observed that the MT at the terminals acts as the transition point, showing that the swallowtail is an interactive phenomenon within the three types of degeneracy lines.

To observe the interactive behaviour and characterize the topology of the degeneracy lines, we realize the non-Hermitian Hamiltonian with a topolectrical circuit, benefiting from a wide range of active circuit devices to accurately control gain and loss and non-reciprocal hoppings. The circuit system can be described by its Laplacian $\mathbf{I}=\boldsymbol{J}\mathbf{V}$, where $\boldsymbol{J}$ denotes the Admittance matrix, $\mathbf{I}$ *is* the vector of input currents, and the output response $\mathbf{V}$ is the vector of node voltages [21]. Obviously, the role of $\boldsymbol{J}$ and its eigenvalues (admittance bands j) play the roles of the Hamiltonian and the energy bands. The circuit element structure is shown in Fig. 1B and part of the designed PCB sample is in Fig. 1C. Hence, the parameter space is replaced by synthetic dimensions, and f_1, f_2 and f_3 become the hopping parameters between the circuit nodes a, b and c. The non-reciprocal hopping between the nodes a and b (and a and c) are implemented precisely by an impedance converter through current inversion (INIC) tandem with capacitors C_1 (C_2). A pure capacitor C_3 simply reveals the reciprocal hopping between b and c. One can properly chose C_1, C_2 and C_3 to implement specific values of f_1, f_2 and f_3. By measuring the voltage responds of each node to a local current input, the admittance eigenvalues and eigenstates can be obtained. More details on experiment are shown in Section 1 of [34]. The swallowtail intersects the plane f_3=0.3 at a spline curve with two cusps (EL3) and an intersection (NIL) (see Fig. 1D) on it, and the corresponding band dispersions (real part) obtained from Eq. (2) (lines) and experimental measurements (circle marks) are shown in Fig. 1E. The presence of the ESs is signified by the quadratic coalescence of two eigenvalues as the parameters vary. Two ESs (one ES is formed by the first and

second bands, and the other is by second and the third bands) intersect at an EL3 (cusp), at which all three eigenvalues are degenerate. Note that the sequence of eigenvalues are sorted from small to large in exact phases. The NIL is an intersection of two nonparallel ESs (both are formed by the second and third bands), which is a linear degeneracy. As f_3 decreases, the enclosed area by the ESs will shrink to the MT on the plane f_3=0.1214 (see Fig. 1F), being a singular point on ES. Observing the band dispersions in Fig. 1G, we discover that the MT is partially a linear degeneracy, but also includes a quadratic coalescence (like an ES). Continuing decreasing f_3, the ESs and the MT will be decoupled into an isolated singularity (i.e. the NL) and a smooth ES (see Fig. 1H for plane f_3=0.01). The NL is a linear degeneracy (similar to the NIL) of the first and the second bands, and the ES is formed by the second and the third bands (see Fig. 1I). The MT plays a role of transition point within different types of degeneracies. The NIL and NL are smoothly connected by the MT, which is tangent to a smoothly connected surface by two different ESs (upper and lower halves are ESs formed by different bands) (see Fig. 1J-K for plane f_1=f_2).

Next, we characterize the topology of the swallowtail with adiabatic transformation of eigenstates. The swallowtail can be formed because the NIL, NL and EL3s are topologically associated with each other. By putting the swallowtail into a sphere (MT at the center, see Fig. 2A), the surfaces and lines of the swallowtail intersect the sphere surface into the geometry in Fig. 2B. Here the cyan lines are ESs, and dots *M*, *N* (blue), *P* and *Q* (black) are NL, NIL and EL3s, respectively, with the regions inside the cyan lines (ESs) being *PT* exact phases, and the outside being the *PT* broken phase region. The adiabatic transformation process of eigenstates is essentially Riemannian geometry (see Sections 2-3 in [34]), and the Lorentz transformation (i.e. SO(2,1) transformation) of eigenstates will result in the polarization (defined by the three components of the eigenstates) conversion of eigenstates as the parameters vary. The NL is the simplest case and is isolated from the ESs. Consider a closed loop circulating the NL (l_1 in Fig. 2B), the eigenvalues return to the initial status with one cycle (see Fig. 2C1), and the eigenstates φ_1, φ_2 and φ_3 of the Hamiltonian rotate (π, π, 0) around the center on the plane defined by the two radial lines (green lines in Fig. 2C2), respectively. Here the bubble plot on the unit sphere shows the evolution process of the polarization direction of the eigenstates, and the increase of bubble size denotes the variation of parameters on the loop. Theoretical and experimental results are consistent with each other as indicated by the upper and lower panels in Fig. 2C2. Since the state assigned by a minus sign is treated as the same state [18] (e.g. rotating $\pm\pi$), the NL carries an integer topological invariant due to the fact that the eigenstates evolve to the initial states.

The NIL and EL3s are hypersurfaces singularities, which are essentially different from the NL. Their topology in exact and broken phases need to be discussed separately, and the corresponding loops are partially located on ESs [30,35]. A closed loop circulating a hypersurface singularities will inevitably traverse ESs, resulting in a hybrid topological invariants [7,30], which is not the focus in this work, and is discussed in Sections 5-6 of [34]. We firstly focus on the exact phases. The NIL is a complete intersection of ESs, and its topology in exact phase is carried by the loop l_2^2. The loop is naturally decomposed into two sub-loops l_2 (basepoint on NIL) by the NIL in the lower and upper regions (see Fig. 2B). Contrary to the NL, the eigenstates φ_2 and φ_3 bifurcate in opposite directions [$\varphi_1 \sim \varphi_3$ rotate (0, $-\pi$, π)]. On the sub-loop l_2, the two eigenstates rotate θ–π and θ respectively, and evolve to antipodal points on the sphere after one cycle (see Fig. 2D2). Such a loop carries a half integer topological invariant (see Section 5 in [34]), because eigenstates do not evolve to the initial states. Cusps are different from complete intersections, and are regarded as the projections of folded curves in higher dimensions in catastrophe theory [28]. The EL3s are exactly formed in the same way, and the ES is folded in view of the 3D space (i.e. j-f_1-f_2, see Fig. 2E1), representing the order exchange of eigenvalues (and the corresponding eigenstates). The topology of the double EL3s in exact phase is characterized by the loop l_3 (Fig. 2A), on which the eigenstates change orders twice, and evolve to the initial states

for one cycle of parameter variation, accompanying the rotation of $(-\pi, 0, \pi)$ for $\varphi_1 \sim \varphi_3$ (see Fig. 2E2). Hence, l_3 carries an integer topological invariant. It can be decomposed into two sub-loops circulating each of the EL3 (Fig. S3 in [34]), on which the eigenstates change orders once and cannot evolve to the initial states, carrying fractional topological invariant (see details in Section 5 of [34]).

In broken phase regions, the NIL is topologically characterized by the loop l_7^2 in Fig. 3A. Different from l_2, the eigenstates φ_2 and φ_3 bifurcate to form a conjugate pair (see Fig. 3E2-E3) on the sub-loop l_7, and evolve to two imaginary vectors in opposite directions (antipodal points on the imaginary sphere, Fig. 3E3) with one cycle. The loop l_7^2 carries an integer topological invariant because φ_2 and φ_3 rotate π and $-\pi$ in complex sphere. The sub-loop l_7 carries a half integer invariant, similar to l_2. The topology of the double EL3s in broken phase is characterized by l_4 (see Fig. 3A). It can be found that the rotation of eigenstates are zero (from Fig. 3B1-B3), and thus l_4 is a trivial loop. The loop l_4 is a product of two nontrivial loops (each circulates a EL3) carrying opposite topological invariants, and both are half integers (see Section 5 of [34]).

We are now ready to discuss the relations of these loops. Previously we showed that φ_2 and φ_3 bifurcate and rotate $\theta-\pi$ and θ on l_2 (Fig. 2D2). However, on loop l_5 (Fig. 3A), being the product of l_2 and l_1, both eigenstates rotate to the same point on the sphere even though they bifurcate on the segment in the gap (see Fig. 3C1-C2). This can be intuitively understood, because the topology of NL provides an additional π rotation to φ_2, adding a minus sign to the final state. Since φ_2 and φ_3 rotate the same angle on l_5, they do not need to bifurcate (contrary to l_2), meaning that it is always possible to stretch l_5 so that it is totally located on ES (l_5' in Fig. 3A). Hence, the NIL is a self-intersection of ES, and the NL plays a role of vortex for bending ES. The two eigenstates can also bifurcate in the complex sphere, meaning that one can continuously stretch l_5' to the broken phase (l_5'' in Fig. 3A). All of the three loops are equivalent to each other, carrying the same topology. The loop l_6 is the product $l_2^{-1}l_3l_4$ (or simply $l_2^{-1}l_3$, l_4 is trivial), on which φ_2 and φ_3 both rotate θ (the same as l_5), and φ_1 rotates $-\pi$ (opposite to l_5). The relation between the two loops is constructed by using l_7. The composite $l_7^{-1}l_5l_7$ (Fig. 3F) can reverse the rotation direction of φ_2 and φ_3 (i.e. $-\theta$), and thus $l_7^{-1}l_5l_7 = l_6^{-1}$, or inversely $l_7^{-1}l_6l_7 = l_5^{-1}$. Hence, as shown in Fig. 3G1, the loop $l_7^{-1}l_5l_7$ ($l_7^{-1}l_6l_7$) can be continuously deformed to l_6^{-1} (l_5^{-1}) without encountering other degeneracy lines, satisfying the topological charge conservation. This relation also ensures two transition processes. The loop $l_3^{-1}l_4$ (Fig. 3G2) enclosing the double EL3s is equivalent to the loop $l_7^{-1}l_5l_7l_2^{-1}$ circulating the NIL and NL, and thus can be continuously deformed to each other. Hence, the double EL3s cannot annihilate each other, but will transit to the NIL and the NL via the MT. The loop l_1 (Fig. 3G3) is equivalent to the loop $l_7l_5^{-1}l_7^{-1}l_2$, so that the NIL and the double EL3s can merge and transit to an NL via the MT. It is understandable that the swallowtail emerges because the degeneracy lines are topologically associated with each other. We provide more data on equivalent loops in Section 7 of [34] that protect the emergence of the swallowtail.

In summary, we have proposed a three-band pseudo-Hermitian system with *PT* symmetry, and discovered that a swallowtail catastrophe singularity emerges in band structures. The swallowtail is an interactive behavior within EL3s, NIL and NL, which was experimentally observed in non-reciprocal circuit. The topology of the degeneracy lines are theoretically and experimentally investigated by adiabatic transformation of eigenstates, showing that they are associated with each other, protecting the

emergence of the swallowtail. Our work introduced the swallowtail catastrophe singularity to the non-Hermitian bands for the first time, enriching the topological classes in non-Hermitian physics. In the future, it is worthwhile to topologically classify systems preserving similar symmetries. Meanwhile, realizing such Hamiltonians in lattice systems could be valuable platforms for investigating finite size effects, e.g. bulk-edge correspondence. The association of singularities of different types possibly open new avenues in sensing and absorbing devices [27,38].

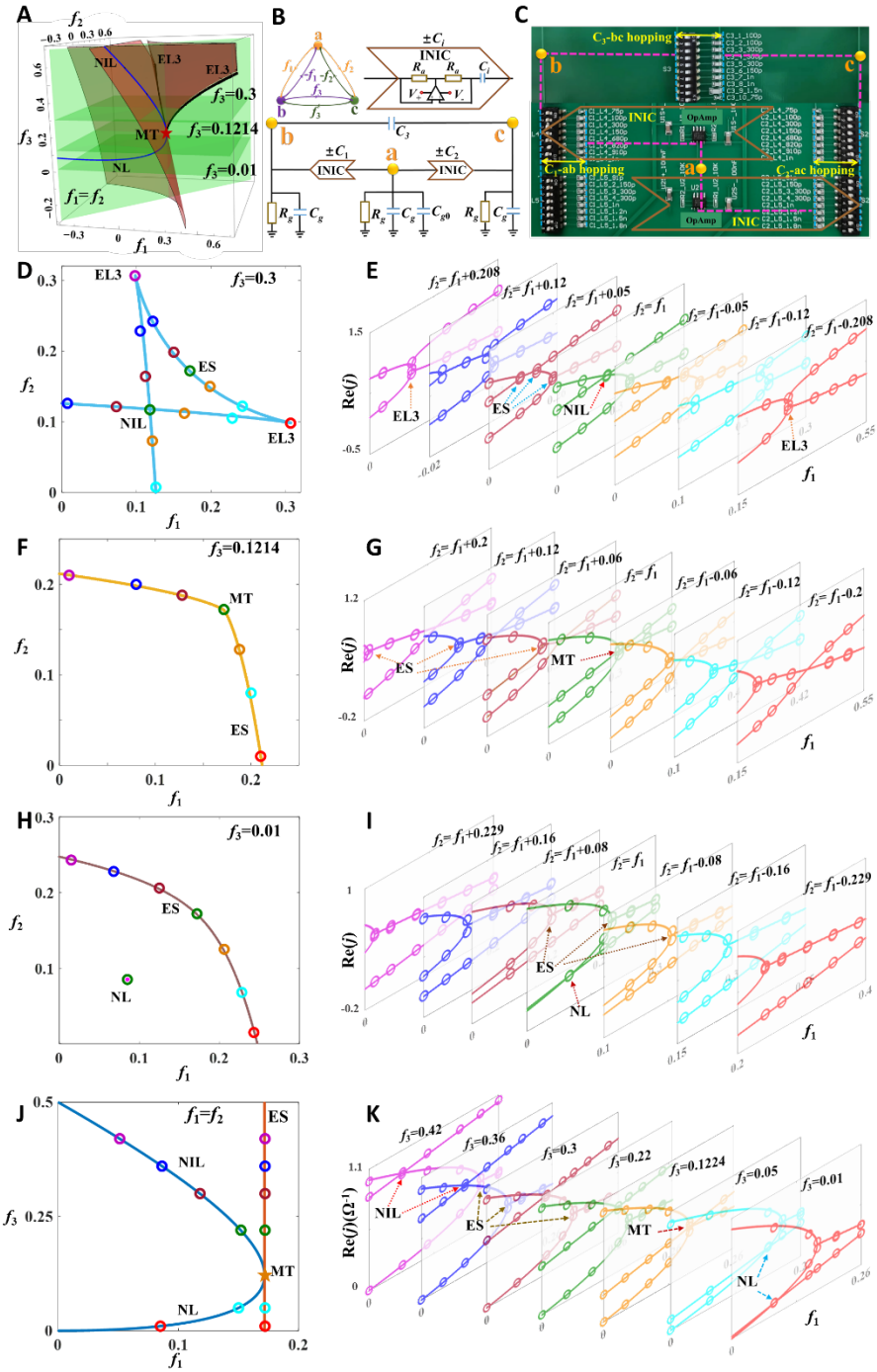

Fig. 1. Observation of swallowtail catastrophe in circuit experiment. (A) Plots of swallowtail in 3D parameter space, obtained by solving zeros of the discriminant of characteristic polynomial of Eq. (2). Red surfaces are ESs, and blue and black lines denote non-defective (NIL and NL) and defective (EL3) degenerate lines. The meeting point (MT) is denoted by the red star. (B) Schematic diagram of the circuit model (composed of three nodes a, b and) realizing the Hamiltonian. Non-reciprocal hoppings are between a and b, and a and c, and reciprocal hopping is between b and c. (C) Picture of the sample. (D-K) Experimental measurement of the swallowtail on planes f_3=0.3 (D-E), f_3=0.1214 (F-G), f_3=0.01 (H-I) and f_1=f_2 (J-K). (D, F, H and J) Degenerate lines and points on the planes. (E, G, I and K) Band structure on the planes. Marks and lines are experimental and theoretical results, respectively.

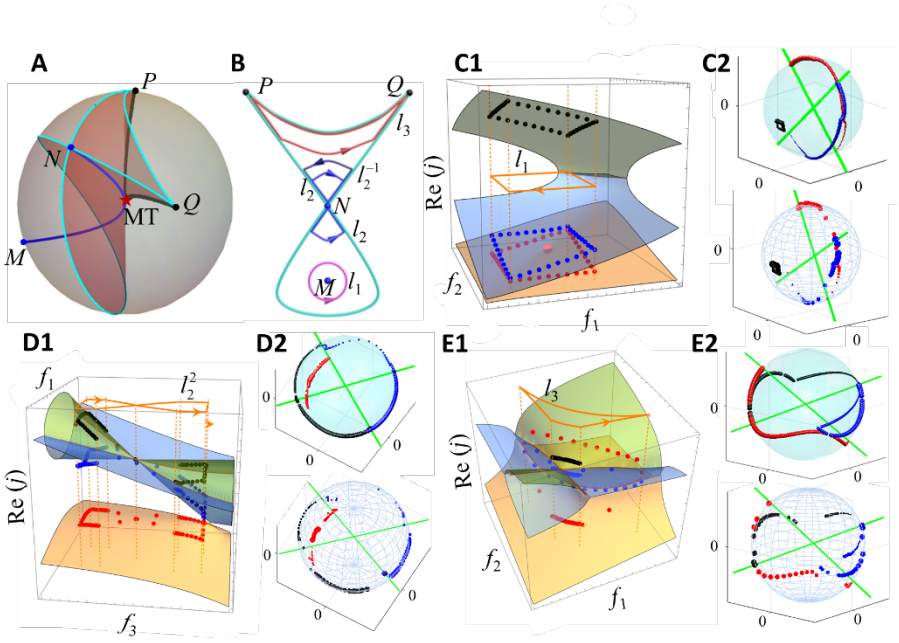

Fig. 2. Loops carrying non-trivial topology in *PT*-exact phases. A. Locating the swallowtail into a sphere, with MT at the center. The ESs intersect the sphere into cyan lines, and EL3s, NIL and NL intersect the sphere into points *P*, *Q*, *N* and *M*, respectively. B. Unfolding the sphere surface (in A) into a plane. Loops l_1 (on plane f_3=0.01), l_2 (on plane f_1+f_2=0.3) and l_3 (on plane f_3=0.3) characterize the topology of NL, NIL and double EL3s in exact phases. l_2 and l_3 are partially on ES, C1-E1. Band structures and evolution of eigenvalues on these loops, with points being experimental results. C2-E2. Adiabatic transformation induced polarization conversion process of eigenstates on these loops. The upper and lower panels are theoretical and experimental results, respectively. The gradually increasing bubble size denotes the evolution process on the loops. Red, blue and black balls in C-E denote φ_1, φ_2 and φ_3 (corresponding eigenvalues: j_1, j_2 and j_3), respectively.

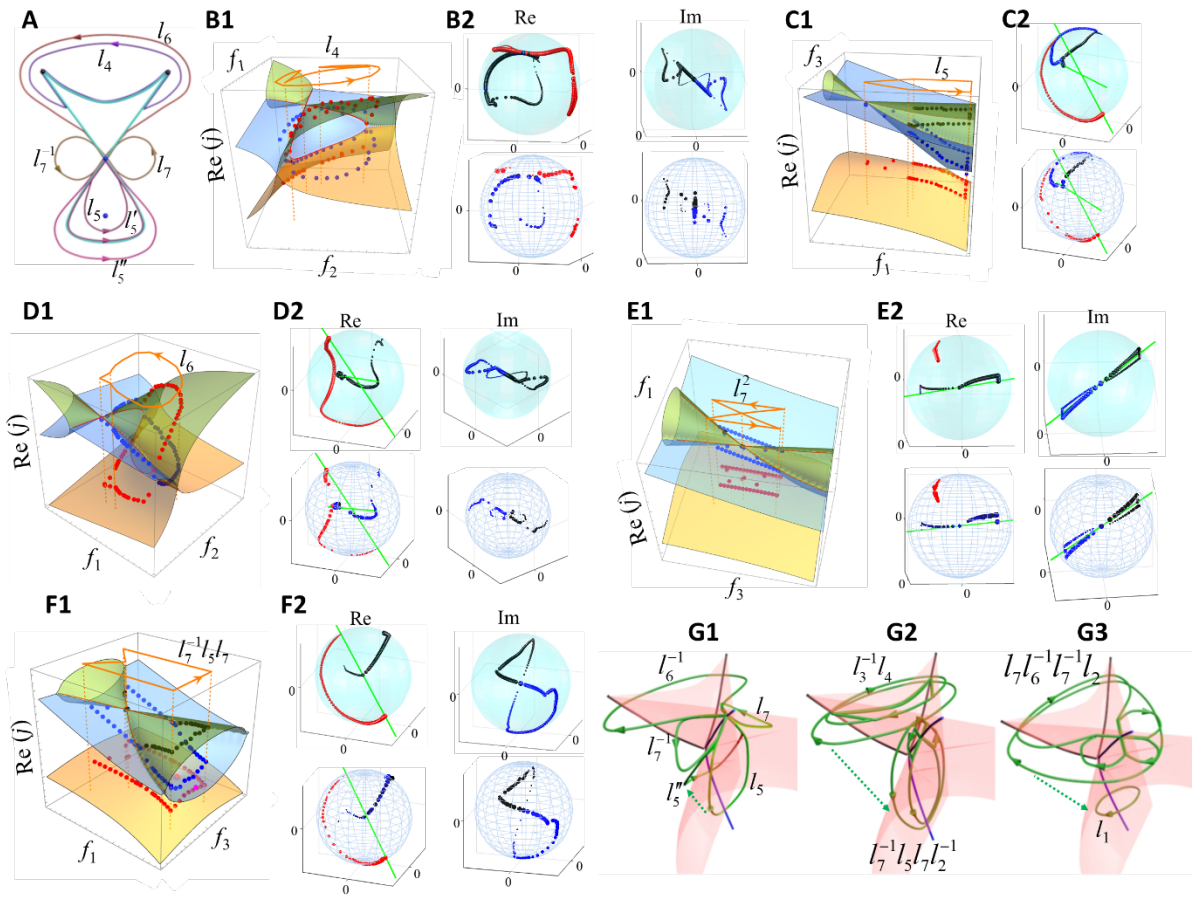

Fig. 3. Topology of NIL and EL3s in broken phases and composite loops. A. l_5 (characterizing NIL in broken phases) and l_7 are on plane f_1+f_2=0.3. l_4 (characterizing NIL in broken phases) and l_6 are on plane f_3=0.3. B1-F1. Evolution of eigenvalues on different loops. D2-F2. Adiabatic transformation induced polarization conversion process on the loops, where Re and Im represent real and imaginary parts of eigenstates. Red, blue and black balls in B-F denote φ_1, φ_2 and φ_3 (corresponding eigenvalues: j_1, j_2 and j_3), respectively. G1-G3. Deformation of loops conserving topological charges. G1. $l_7^{-1}l_5l_7$ can be deformed to l_6^{-1} by stretching l_5 to l_5'' and opening the basepoint. G2. The loop $l_3^{-1}l_4$ that encloses the double EL3s can be deformed to $l_7^{-1}l_5l_7l_2^{-1}$, which circulates the NIL and NL. G3. The loop $l_5l_6^{-1}l_7^{-1}l_2$ (circulating the NIL and the double EL3s) can be deformed to l_1 (circulating the NL).

References:

1. Kawabata K, Shiozaki K, Ueda M, et al. Symmetry and topology in non-Hermitian physics[J]. Physical Review X, 2019, 9(4): 041015.
2. Zhou H, Peng C, Yoon Y, et al. Observation of bulk Fermi arc and polarization half charge from paired exceptional points[J]. Science, 2018, 359(6379): 1009-1012.
3. Lai Y H, Lu Y K, Suh M G, et al. Observation of the exceptional-point-enhanced Sagnac effect[J]. Nature, 2019, 576(7785): 65-69.
4. Kawabata K, Bessho T, Sato M. Classification of exceptional points and non-Hermitian topological semimetals[J]. Physical review letters, 2019, 123(6): 066405.
5. Miri M A, Alu A. Exceptional points in optics and photonics[J]. Science, 2019, 363(6422): eaar7709.
6. Bergholtz E J, Budich J C, Kunst F K. Exceptional topology of non-Hermitian systems[J]. Reviews of Modern Physics, 2021, 93(1): 015005.
7. Tang W, Jiang X, Ding K, et al. Exceptional nexus with a hybrid topological invariant[J]. Science, 2020, 370(6520): 1077-1080.
8. Shen H, Zhen B, Fu L. Topological band theory for non-Hermitian Hamiltonians[J]. Physical review letters, 2018, 120(14): 146402.
9. Wan X, Turner A M, Vishwanath A, et al. Topological semimetal and Fermi-arc surface states in the electronic structure of pyrochlore iridates[J]. Physical Review B, 2011, 83(20): 205101.
10. Burkov A A, Hook M D, Balents L. Topological nodal semimetals[J]. Physical Review B, 2011, 84(23): 235126.
11. Burkov A A, Balents L. Weyl semimetal in a topological insulator multilayer[J]. Physical review letters, 2011, 107(12): 127205.
12. Lu L, Fu L, Joannopoulos J D, et al. Weyl points and line nodes in gyroid photonic crystals[J]. Nature photonics, 2013, 7(4): 294-299.
13. Soluyanov A A, Gresch D, Wang Z, et al. Type-ii weyl semimetals[J]. Nature, 2015, 527(7579): 495-498.
14. Young S M, Kane C L. Dirac semimetals in two dimensions[J]. Physical review letters, 2015, 115(12): 126803.
15. Chiu C K, Teo J C Y, Schnyder A P, et al. Classification of topological quantum matter with symmetries[J]. Reviews of Modern Physics, 2016, 88(3): 035005.
16. Yang B, Guo Q, Tremain B, et al. Ideal Weyl points and helicoid surface states in artificial photonic crystal structures[J]. Science, 2018, 359(6379): 1013-1016.
17. Jia H, Zhang R, Gao W, et al. Observation of chiral zero mode in inhomogeneous three-dimensional Weyl metamaterials[J]. Science, 2019, 363(6423): 148-151.
18. Wu Q S, Soluyanov A A, Bzdušek T. Non-Abelian band topology in noninteracting metals[J]. Science, 2019, 365(6459): 1273-1277.
19. Guo Q, Jiang T, Zhang R Y, et al. Experimental observation of non-Abelian topological charges and edge states[J]. Nature, 2021, 594(7862): 195-200.

20. Okuma N, Kawabata K, Shiozaki K, et al. Topological origin of non-Hermitian skin effects[J]. Physical review letters, 2020, 124(8): 086801.

21. Helbig T, Hofmann T, Imhof S, et al. Generalized bulk–boundary correspondence in non-Hermitian topolectrical circuits[J]. Nature Physics, 2020, 16(7): 747-750.

22. Yao S, Wang Z. Edge states and topological invariants of non-Hermitian systems[J]. Physical review letters, 2018, 121(8): 086803.

23. Song F, Yao S, Wang Z. Non-Hermitian skin effect and chiral damping in open quantum systems[J]. Physical review letters, 2019, 123(17): 170401.

24. Zhang K, Yang Z, Fang C. Correspondence between winding numbers and skin modes in non-Hermitian systems[J]. Physical Review Letters, 2020, 125(12): 126402.

25. Zhang X, Ding K, Zhou X, et al. Experimental observation of an exceptional surface in synthetic dimensions with magnon polaritons[J]. Physical Review Letters, 2019, 123(23): 237202.

26. Okugawa R, Yokoyama T. Topological exceptional surfaces in non-Hermitian systems with parity-time and parity-particle-hole symmetries[J]. Physical Review B, 2019, 99(4): 041202.

27. Zhong Q, Ren J, Khajavikhan M, et al. Sensing with exceptional surfaces in order to combine sensitivity with robustness[J]. Physical review letters, 2019, 122(15): 153902.

28. Arnol'd V I. Catastrophe theory[M]. Springer Science & Business Media, 2003.

29. Yixin paper

30. My paper

31. Kirillov O N, Overton M. Robust stability at the swallowtail singularity[J]. Frontiers in Physics, 2013, 1: 24.

32. Raz O, Pedatzur O, Bruner B D, et al. Spectral caustics in attosecond science[J]. Nature Photonics, 2012, 6(3): 170-173.

33. Pierre Delplace, Tsuneya Yoshida, and Yasuhiro Hatsugai, Symmetry-Protected Multifold Exceptional Points and Their Topological Characterization. PRL 2021

34. Supplementary material

35. Hoeller J, Read N, Harris J G E. Non-Hermitian adiabatic transport in spaces of exceptional points[J]. Physical Review A, 2020, 102(3): 032216.

36. Chandrasekaran A, Shtyk A, Betouras J J, et al. Catastrophe theory classification of fermi surface topological transitions in two dimensions[J]. Physical Review Research, 2020, 2(1): 013355.

37. Yuan N F Q, Fu L. Classification of critical points in energy bands based on topology, scaling, and symmetry[J]. Physical Review B, 2020, 101(12): 125120.

38. Soleymani S, Zhong Q, Mokim M, et al. Chiral and degenerate perfect absorption on exceptional surfaces[J]. Nature communications, 2022, 13(1): 1-8.